References and Notes

1. S. A. Maier *et al.*, *Nat. Mater.* **2**, 229 (2003).
2. J. Hoinville *et al.*, *J. Appl. Phys.* **93**, 7187 (2003).
3. J. Grunes, J. Zhu, E. A. Anderson, G. A. Somorjai, *J. Phys. Chem. B* **106**, 11463 (2002).
4. M. Zayats *et al.*, *J. Am. Chem. Soc.* **125**, 16006 (2003).
5. A. E. Saunders, B. A. Korgel, *ChemPhysChem* **6**, 61 (2005).
6. F. X. Redl, K. S. Cho, C. B. Murray, S. O'Brien, *Nature* **423**, 968 (2003).
7. A. L. Rogach, *Angew. Chem. Int. Ed.* **43**, 148 (2004).
8. E. V. Shevchenko, D. V. Talapin, N. A. Kotov, S. O'Brien, C. B. Murray, *Nature* **439**, 55 (2006).
9. M. E. Leunissen *et al.*, *Nature* **437**, 235 (2005).
10. B. A. Grzybowski, A. Winkleman, J. A. Wiles, Y. Brumer, G. M. Whitesides, *Nat. Mater.* **2**, 241 (2003).
11. J. Kolny, A. Kornowski, H. Weller, *Nano Lett.* **2**, 361 (2002).
12. For crystals composed of Ag and Au nanoparticles, the lattice is isostructural with sphalerite ZnS (SG 216). For crystals made of only one type of metal cores (compare Fig. 5B), the lattice is best described as diamond (SG 227). To account for both of these possibilities we use "diamond-like" nomenclature in the text.
13. D. Witt, R. Klajn, P. Barski, B. A. Grzybowski, *Curr. Org. Chem.* **8**, 1763 (2004).
14. N. R. Jana, X. G. Peng, *J. Am. Chem. Soc.* **125**, 14280 (2003).
15. Supporting material is available on *Science* Online.
16. C. V. K. Sharma, G. A. Broker, G. J. Szulczewski, R. D. Rogers, *Chem. Commun.* **2000**, 1023 (2000).
17. After the evaporation of the "good" solvent, the NP crystals constituted only ~0.01% v/v of the remaining solution, so crystallization cannot be attributed to confinement effects that might have been operative had all liquid been evaporated.
18. S. Link, Z. L. Wang, M. A. El-Sayed, *J. Phys. Chem. B* **103**, 3529 (1999).
19. This estimate is based on the Deryagin-Landau-Verwey-Overbeek (DLVO) theory and for a 1:1 electrolyte. Specifically, $\kappa_C^{-1} = (\varepsilon\varepsilon_0 k_B T/2ce^2)^{1/2}$, where c denotes the number density of ions, e is the charge of an electron, ε is the static dielectric constant of the medium, and ε_0 is the permittivity of vacuum. Using EDS, we determined the content of Cl^- to be ~5%, which corresponds to a concentration $c \sim 10^{-2}$ M of the residual ammonium salt ($NMe_4^+Cl^-$) present in the crystal. Assuming that the effective dielectric constant of a mixture of water and DMSO filling the free space between the NPs in the crystal can be approximated as $\varepsilon_{eff} = (\varepsilon_{water} + \varepsilon_{DMSO})/2 \approx 65$, $\kappa_C^{-1} \sim 2.7$ nm. We emphasize that this number can only be treated as an estimate, because with NPs several nanometers in diameter, we are at the limit of applicability of the DLVO mean-field approach. At the same time, our approximation is qualitatively correct as verified by recent numerical Monte Carlo simulations of pairs of nanometer-sized charged particles (*20*).
20. J. Z. Wu, D. Bratko, H. W. Blanch, J. M. Prausnitz, *J. Chem. Phys.* **111**, 7084 (1999).
21. C. Kittel, *Introduction to Solid State Physics* (Wiley, Hoboken, NJ, ed. 8, 2005).
22. J. N. Israelachvili, *Intermolecular and Surface Forces* (Academic Press, San Diego, ed. 2, 1992).
23. A.-P. Hynninen, M. E. Leunissen, A. van Blaaderen, M. Dijkstra, *Phys. Rev. Lett.* **96**, 018303 (2006).
24. P. Ziherl, R. D. Kamien, *J. Phys. Chem. B* **105**, 10147 (2001).
25. Because each NP is covered with a SAM, the only dispersion (van der Waals) interaction that needs to be considered is that between alkyl chains of MUA and TMA thiols that form the SAMs. This attractive interaction is important only if the SAMs interpenetrate; it vanishes at distances larger than ~1 nm, and its characteristic energy—assuming ideal parallel alignment of two alkyl chains—is on the order of k_BT per CH_2 group (*26*, *27*). TEM images of the charged NPs that we used reveal that the SAMs are "rigid" (i.e., their thicknesses between aggregated NPs are the same as those on isolated ones) and that no interpenetration takes place. This observation is easily rationalized by noting that possible interpenetration of the alkyl chains would have to take place at the expense of favorable electrostatic interactions between oppositely charged head groups. Overall, the van der Waals forces in our system can be neglected even if two NPs touch each other. At such small separations, the interactions are dominated by attractive electrostatic forces. Finally, we note that entropic forces due to SAM squeezing (*28*) are also negligible, because the SAMs are not "compressible."
26. L. Salem, *J. Chem. Phys.* **37**, 2100 (1962).
27. C. D. Bain *et al.*, *J. Am. Chem. Soc.* **111**, 321 (1989).
28. P. Ziherl, R. D. Kamien, *Phys. Rev. Lett.* **85**, 3528 (2000).
29. Results of recent molecular dynamics simulations (*21*) indicate that mean-field screening concepts can be extended to the nanoscale and can be used to approximate electrostatic forces acting between nanoparticles screened by counterions comparable in size (within one order of magnitude) and present in small quantities (a few layers). Although quantitative analogies could thus be justified, we restrict our discussion to qualitative arguments that are sufficient to explain experimental observations.
30. V. Tohver, J. E. Smay, A. Braem, P. V. Braun, J. A. Lewis, *Proc. Natl. Acad. Sci. U.S.A.* **98**, 8950 (2001).
31. M. Rasa, A. P. Philipse, J. D. Meeldijk, *J. Colloid Interface Sci.* **278**, 115 (2004).
32. R. C. Ball, D. A. Weitz, T. A. Witten, F. Leyvraz, *Phys. Rev. Lett.* **58**, 274 (1987).
33. P. C. Ohara, D. V. Leff, J. R. Heath, W. M. Gelbart, *Phys. Rev. Lett.* **75**, 3466 (1995).
34. P. M. Chaikin, T. C. Lubensky, *Principles of Condensed Matter Physics* (Cambridge Univ. Press, Cambridge, ed. 1, 2000).
35. S. Sanyal, N. Easwar, S. Ramaswamy, A. K. Sood, *Europhys. Lett.* **18**, 107 (1992).
36. J. Lyklema, *Fundamentals of Interface and Colloid Science* (Academic Press, London, San Diego, 1995).
37. E. J. W. Verwey, J. T. G. Overbeek, *Theory of the Stability of Lyophobic Colloids* (Dover, Mineola, NY, 1999).
38. Z. Zhang, A. S. Keys, T. Chen, S. C. Glotzer, *Langmuir* **21**, 8383 (2005).
39. S. Stoeva, K. J. Klabunde, C. M. Sorensen, I. Dragieva, *J. Am. Chem. Soc.* **124**, 2305 (2002).

40. We thank J.-G. Zheng and M. Kowski for helpful discussions. B.A.G. gratefully acknowledges financial support from the Camille and Henry Dreyfus New Faculty Awards Program, NSF (grant 0503673), and the American Chemical Society Petroleum Research Fund (Award 42953-AC5). K.J.M.B. was supported by the NSF Graduate Fellowship.

Supporting Online Material

www.sciencemag.org/cgi/content/full/1125124/DC1
Materials and Methods
Figs. S1 and S2
References and Notes

18 January 2006; accepted 8 February 2006
Published online 23 February 2006;
10.1126/science.1125124
Include this information when citing this paper.

Downloaded from http://science.sciencemag.org/ on November 19, 2019

Probing Proton Dynamics in Molecules on an Attosecond Time Scale

S. Baker,[1] J. S. Robinson,[1] C. A. Haworth,[1] H. Teng,[1] R. A. Smith,[1] C. C. Chirilă,[2] M. Lein,[2] J. W. G. Tisch,[1] J. P. Marangos[1]*

We demonstrate a technique that uses high-order harmonic generation in molecules to probe nuclear dynamics and structural rearrangement on a subfemtosecond time scale. The chirped nature of the electron wavepacket produced by laser ionization in a strong field gives rise to a similar chirp in the photons emitted upon electron-ion recombination. Use of this chirp in the emitted light allows information about nuclear dynamics to be gained with 100-attosecond temporal resolution, from excitation by an 8-femtosecond pulse, in a single laser shot. Measurements on molecular hydrogen and deuterium agreed well with calculations of ultrafast nuclear dynamics in the H_2^+ molecule, confirming the validity of the method. We then measured harmonic spectra from CH_4 and CD_4 to demonstrate a few-femtosecond time scale for the onset of proton rearrangement in methane upon ionization.

There is currently great interest in the development of methods to probe the dynamical behavior of matter on the attosecond (1 as = 10^{-18} s) time scale (*1*–*3*). It is known that the ionization of an atom or molecule by an intense laser field and subsequent electron acceleration in the field results in the formation of a chirped electron wavepacket—a "burst" of electrons with a broad range of kinetic energies that recollide with the parent ion over a range of time delays (*4*). However, the chirp of the electron wavepacket is a hitherto unexploited property in the measurement of ultrafast dynamical behavior.

The technique demonstrated here is based on high-harmonic generation (HHG) from molecules. HHG is well understood within the framework of a semiclassical model (*5*), which separates the process into three distinct steps. In the first step, an intense laser pulse ionizes an atom or molecule, launching an electron wavepacket into the continuum. In the next step, the electron wavepacket moves in response to the laser electric field; it is first accelerated away from the parent ion and then returns at some later time (typically 0.5 to 1.6 fs for a laser field at a wavelength of ~800 nm) as the laser field reverses direction. The third step is the recombination of the electron with the parent ion and the emission of a high-energy photon (~10 to 500 eV) that carries away, at discrete multiples of the laser frequency (*6*), the kinetic energy gained by the electron in the process.

The intensity of the radiation emitted at the moment of recombination depends upon the transition amplitude between the wave function de-

[1]Blackett Laboratory, Imperial College London, Prince Consort Road, South Kensington, London SW7 2BZ, UK. [2]Max Planck Institute for Nuclear Physics, Saupfercheckweg 1, 69117 Heidelberg, Germany.

*To whom correspondence should be addressed. E-mail: j.marangos@imperial.ac.uk

scribing the electron and ion at this instant and the initial molecular ground state. Lein (*7*) showed theoretically that the harmonic signal in a molecule will be approximately proportional to the squared modulus of the nuclear autocorrelation function, which is the overlap between the initial and final nuclear parts of the molecular wave function that evolves from the moment of ionization until the point of recollision. Details of the nuclear dynamics are therefore encoded in the HHG signal, which is blind to all other competing channels because the quantum mechanical path for the molecule starts and ends in the same state.

Our method (Fig. 1) can be viewed as a pump-probe technique. The ionization step of harmonic emission is the pump, because in the case of a molecule, a nuclear wavepacket is simultaneously launched at the moment of ionization. The probe is the recollision of the electron wavepacket with the parent ion, with the nuclear wavepacket information encoded in the emitted harmonics.

The use of the recollision as a probe is broadly related to earlier experiments by Niikura *et al*., who used the correlation of electron and nuclear wavepackets (*1*, *2*) to provide information about the instantaneous average internuclear separation with subfemtosecond temporal resolution. In that work, the kinetic energy released in recollision-induced fragmentation was used for the probe signal, and thus the temporal resolution was limited to >0.5 fs by the inherent temporal spread of the recolliding electron bunch. A further limitation was the requirement to tune the laser wavelength over a wide range to vary the pump-probe delays. The kinetic energy release technique has so far been restricted to observing motion along the internuclear axis of diatomic molecules; it is also affected by competing excitation channels. In contrast, our method measures the quantum mechanical nuclear dynamics by determining the overlap integral between the wave function at two times, so it is sensitive to motion in any direction. Further, by using the chirp associated with harmonic emission (*4*) to probe the nuclear motion, we attain ~100-as time resolution as well as access to a range of pump-probe time delays for a single laser pulse at fixed wavelength.

The high temporal resolution available in our technique arises from the chirped nature of the recolliding electron wavepacket (Fig. 2). Electrons born into the continuum between ~1/20th of an optical cycle after the laser field maximum and the next zero of the field follow so-called "short trajectories" (*8*) that return quickly to the core. Each of these short trajectories returns to the parent ion at a different delay time Δt, and each is associated with a different electron kinetic energy at the point of recollision. This temporal spread leads to a frequency-chirped harmonic emission, with successively higher harmonics being generated at longer time delays, as has been directly measured by Mairesse *et al*. (*4*). This property of HHG is fundamental to the technique demonstrated here, because it allows a range of pump-probe delays to be accessed by analysis of a single harmonic spectrum. In principle, a second set of longer trajectories can contribute to the HHG spectrum, with the electron born earlier and returning later to the core, but in this experiment these long trajectories are filtered out from the spectrum, yielding a one-to-one mapping between delay and photon frequency (Fig. 2). Simply recording the harmonic spectrum therefore allows us to probe the nuclear motion over a range of pump-probe time delays set by the temporal spread of the recolliding electron wavepacket.

We implement this method by observing the ratio of the harmonic spectra generated in gaseous H_2 and D_2, or CH_4 and CD_4. The use of isotopes ensures that the variation in HHG spectra is due primarily to differing nuclear dynamics, because the electronic states are very similar. The variation of this ratio with harmonic order then yields information concerning the differing nuclear (proton or deuteron) dynamics in the ions of the two species, with the 100-as time resolution encoded in the frequency of the emitted radiation over a range of ~1 fs for laser light of ~800 nm wavelength. The HHG efficiency decreases more over a given range of harmonic orders for H_2 than for D_2 because of faster nuclear motion in the lighter molecule.

We used very short laser pulses in this experiment to freeze rotational motion. We generated 8-fs pulses centered at a wavelength of ~775 nm with the use of a gas-filled hollow fiber and chirped mirrors to compress ~0.75-mJ, 30-fs pulses. The laser beam was focused by an off-axis paraboloid mirror (focal length 400 mm) into a pulsed gas jet (Fig. 1A). The focus was located 9 mm before the gas jet to ensure that short electron trajectories dominated the harmonic signal. The intensity at the interaction region was estimated to be 2×10^{14} W cm^{-2}. The harmonic signal was spectrally dispersed in a grazing-incidence, angularly resolving, flat-field spectrometer and was detected by an extreme ultraviolet–sensitive imaging microchannel plate detector, with a charge-coupled device (CCD) camera used for readout. The harmonic spectrum was extracted by angular integration of the CCD images. Because the first ionization potential in the two species is very similar [15.43 eV for H_2, 15.46 eV for D_2 (*9*)], differences in phase-matching conditions for harmonic generation in the two cases were negligible: The harmonics generated in H_2 and D_2 had identical far-field angular distributions.

It was essential that each gas (e.g., H_2 or D_2) was delivered to the interaction region at an equal

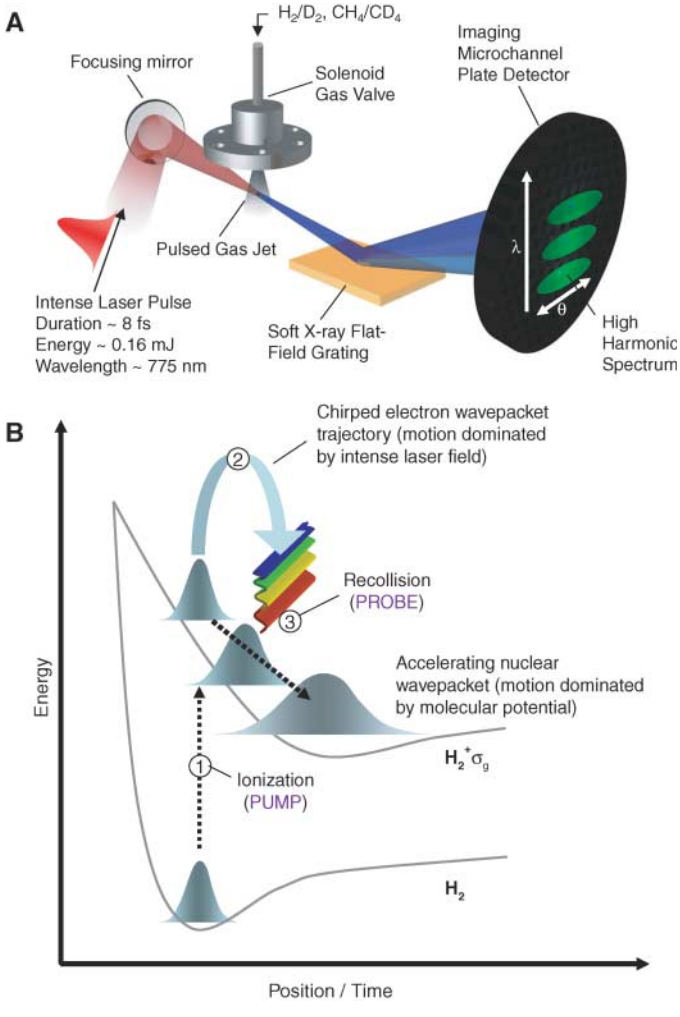

Fig. 1. Pump-probe method for measuring proton dynamics in molecules. (**A**) The experimental setup required to observe high-harmonic emission. (**B**) Ionization serves as the pump process because it launches an electron wavepacket into the continuum simultaneously with a nuclear wavepacket on the H_2^+ ground state potential surface (σ_g). The electron wavepacket then moves in response to the laser field, returning to the parent ion with an increased kinetic energy at some later time. The recollision acts as the probe of the nuclear motion that has occurred in the time delay since ionization occurred.

Downloaded from http://science.sciencemag.org/ on November 19, 2019

density. We ensured this condition by using a high-intensity, 800-fs laser field at 1053 nm to fully ionize the gas, and performing interferometric measurements and Abel inversion to characterize the electron density. The experimentally determined backing pressure ratio, $P(D_2)/P(H_2)$, that was found to equalize the electron (and therefore molecular) density was 1.3 ± 0.1. This ratio was measured with a species-independent piezoelectric gauge in the gas jet backing line and agrees, within experimental error, with gas flow calculations and other tests based on the pressure jump in the interaction chamber after pulsing the valve a fixed number of times with the vacuum pumps off.

Typical high-harmonic spectra from H_2 and D_2 at equal density are shown in Fig. 3A. Spectra were averaged over 400 laser shots, although it should be noted that the full dynamical information is encoded in each spectrum recorded. In agreement with Lein's predictions, Fig. 3A shows that the harmonic signal at all orders detected is higher in D_2 than in H_2—a clear signature of the slower nuclear motion occurring in D_2. As expected from the different speeds of nuclear motion, we see a significant increase in the D_2/H_2 HHG intensity ratio as the frequency of the harmonic, and therefore the time delay, increases (Fig. 3B).

We compared our experimental results with a calculation based on the strong-field approximation, which collects the effect of the nuclear motion in the compact nuclear correlation function (*10*). The harmonics are approximately proportional to the squared modulus of the nuclear autocorrelation function, $c(\tau) = \int \chi(R,0)\chi(R,\tau)dR$, where $\chi(R,0)$ and $\chi(R,\tau)$ are the initial and propagated vibrational wavepackets in the molecular ion, R is the internuclear distance, and τ is the electron travel time (equivalent to our delay time, Δt). For geometrical reasons, most of the molecules in the randomly aligned sample in our experiment have their molecular axes nearly perpendicular to the laser electric field direction, which reduces the effect of two-center interference (*11*) and minimizes Stark shifts (*12*). We have confirmed in test calculations that the influence of the Stark shifts in the Born-Oppenheimer potential is negligible for the present set of parameters. Two-center interference gives rise to a small but clearly discernable shift and has been included in our analysis. For random orientation, this effect can be taken into account by using the nuclear correlation function $c(\tau,k) = \int \chi(R,0)\chi(R,\tau)f(k,R)dR$ including the interference kernel $f(k,R) = \sin(kR/2)/(kR/2)$. Here, k is the wave vector of the recolliding electron, evaluated using the relation $\hbar^2k^2/(2m) = \hbar\omega$ (*13*), where $\hbar$ is Planck's constant divided by 2π, and $\hbar\omega$ is the energy of the harmonic being emitted upon recombination. The ratio of harmonic intensities D_2/H_2 is calculated by taking the ratio of the squared modulus of the two correlation functions for D_2 and H_2. The calculated curve is scaled to account for the slight difference in photoionization cross sections for H_2 and D_2 (*14*). We found good quantitative agreement between our measurements and the calculation (Fig. 3B).

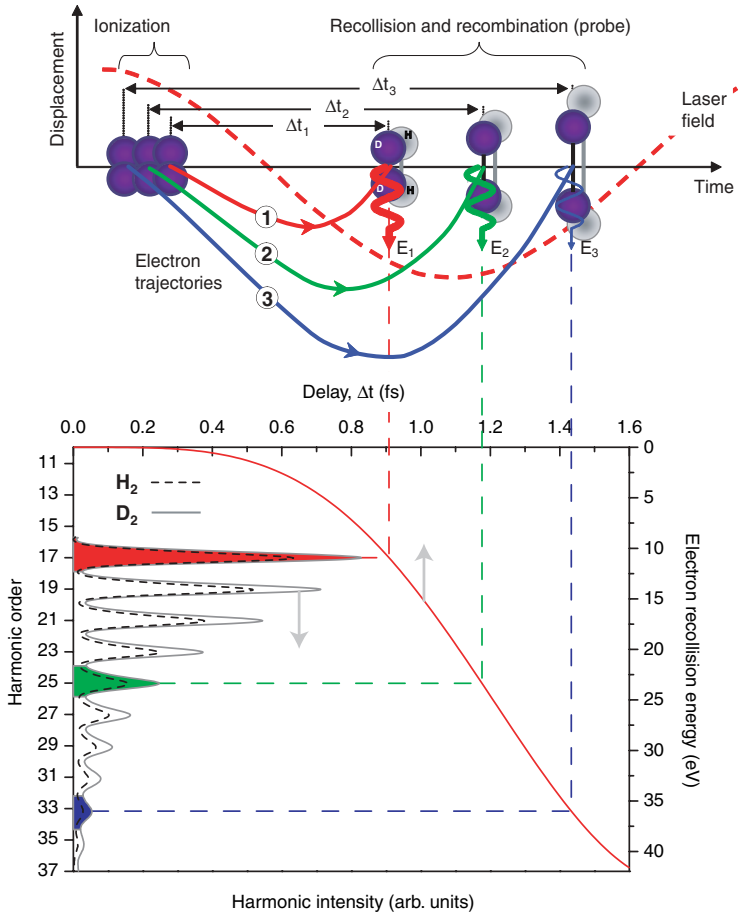

Fig. 2. Encoding of nuclear dynamics within harmonic spectra. Upper panel: The trajectory of the ionized electron differs depending on the exact time of ionization. Three possible electron trajectories labeled 1, 2, and 3 are shown, which recollide with the molecular ion after delays Δt_1, Δt_2, and Δt_3, with increasing kinetic energy E_1, E_2, and E_3, resulting in the emission of increasingly higher frequency photons after recombination (shown as the 17th, 25th, and 33rd harmonics for the purpose of this illustration). Note: Although the curves in the lower panel are physically accurate, the electron trajectories shown in the upper panel have been slightly altered to improve clarity.

The nuclear wave function $\chi(R,t)$ and, from this, the time evolution of the expectation value of R [$\langle R(t)\rangle$)] in each molecule was reconstructed from the recorded intensity spectra and their ratio by use of a genetic algorithm (*7*, *10*). Agreement with the exact calculation is good (Fig. 3C). Therefore, the measurement of the harmonic spectrum ratio can be used to determine proton (deuteron) motion in H_2 and D_2 molecules ~1 fs after ionization, with a temporal resolution of ~100 as (the difference in recollision times between successive harmonic orders). Here we use the data from H_2/D_2 primarily to test and confirm the method, as the potential surface and thus the calculated dynamics of the proton are known in the case of H_2. Therefore, the agreement between the measurement and the calculated ratio of the nuclear correlation function (Fig. 3B) is confirmation that the chirp of the electron is satisfactorily given by the semiclassical treatment, validating the frequency-to-time mapping. With this confirmation, we can apply the technique to other molecules for which the potentials are not fully known.

The HHG spectrum is determined by the squared moduli of $c(\tau)$ and of the remaining parts $\bar{d}(\omega)$ of the transition dipole moment that do not depend on the nuclear motion. Similar to Itatani *et al.* (*15*), we write $\bar{d}(\omega) = a[k(\omega)]r[k(\omega)]$, where $a[k(\omega)]$ is the amplitude for an electron of wave vector k, and $r[k(\omega)]$ is the recombination part of $\bar{d}(\omega)$. It is feasible to directly calibrate the factor $\bar{d}(\omega)$ by measuring a given harmonic over a range of laser intensities (so that $r[k(\omega)]$ would be fixed but the recollision time would be changing with laser intensity). An auxiliary measurement on an atom of similar ionization potential would be used to establish the variation of $a[k(\omega)]$ with recollision time. In our implementation of the method, the equivalence of $\bar{d}(\omega)$ for the protonated and deuterated species has been used to remove the spectral variation of this factor. This simplification is experimentally convenient, as then the main technical difficulty is simply to ensure equal particle densities in the comparison, with only a single set of measurements being required at a fixed and known laser intensity.

Downloaded from http://science.sciencemag.org/ on November 19, 2019

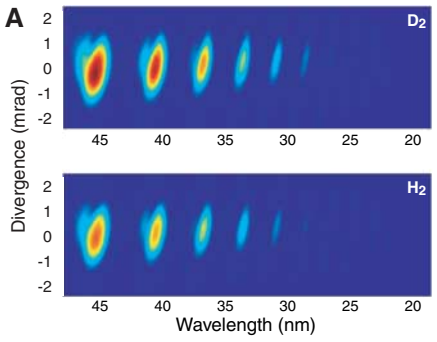

Fig. 3. Harmonic emission in H_2 and D_2. **(A)** Raw CCD images on a common intensity scale (red represents brightest signal, blue weakest) revealing that at all orders observed, harmonic emission is weaker in H_2 than in D_2 at the same density. **(B)** Ratio of harmonic peak intensities for D_2 and H_2 (black). Vertical errors represent SEM for 400 laser shots. Horizontal errors are estimated from quantum mechanical energy-time uncertainty. The control ratio of two harmonic spectra from H_2 taken separately is also shown (red) and is seen to be unity for all harmonic orders, as expected. The blue line is a calculation of harmonic ratio (described in text). **(C)** The nuclear motion reconstructed from the experimental data by multiple runs of a genetic algorithm (red curves) converges closely to the exact result (blue curves) calculated using the exact Born-Oppenheimer potentials for H_2^+ and D_2^+.

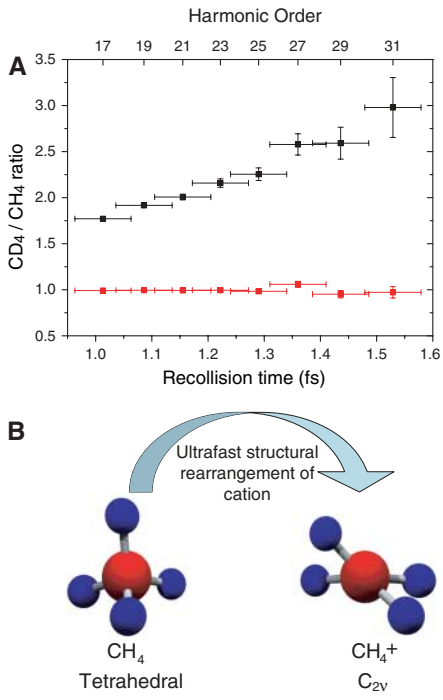

Fig. 4. Probing structural rearrangement in CH_4 and CD_4. **(A)** Ratio of harmonic signals in CD_4 and CH_4 (black). The error represents SE over 200 laser shots. Also shown is the control ratio of two harmonic spectra from CD_4 taken separately (red). **(B)** Known structures of CH_4 and CH_4^+ at equilibrium. Upon removal of an electron, it is anticipated that CH_4 will rapidly evolve toward the CH_4^+ structure shown.

To further explore the application of this technique, we compared harmonic spectra obtained in CH_4 and CD_4 (Fig. 4A). We observed behavior consistent with our studies of D_2 and H_2: The harmonic yield is found to be greater in the heavier isotope whose nuclei are expected to move more slowly, and this effect is found to be enhanced for the higher order harmonics, which probe the parent molecule at a longer time delay. The differing photoabsorption cross sections in CH_4 and CD_4 (*16*), although making a small contribution to the measured ratio, cannot account for the increase in the ratio that we observe. These results therefore confirm that this technique is not limited to probing nuclear wavepackets in diatomic molecules.

It is known from theory (*17*) and experiment (*18*, *19*) that although the CH_4 molecule has the well-known tetrahedral structure (with 109.50° bond angles), CH_4^+ adopts a C_{2v} geometry, with some bond angles diminishing to <60° (Fig. 4B). It is anticipated that these structural rearrangements at the moment of ionization must be fast, as the tetrahedral structure of methane is far from the equilibrium bond angles of the ion. Our measurements provide direct evidence that the time scale for the onset of this structural rearrangement is on the order of a few femtoseconds. The measured ratio (Fig. 4A) is the square of the ratio of the nuclear autocorrelation functions for the two species, a quantity that can be calculated directly from the molecular potentials. Therefore, the measurement can be used to test the correctness of computed potentials.

Several extensions of the technique are possible. Use of a driving laser field of a longer wavelength would extend the time window over which information on the nuclear dynamics can be gained; for instance, a field at a wavelength of 2 μm would allow motion to be followed for up to 4 fs after ionization. This could also be achieved by selection of the long-trajectory component of the chirped electron wavepacket for harmonic emission without affecting the temporal resolution of the measurement. A further extension of the technique may be to study neutral molecular dynamics by starting from negative molecular ions formed through electron attachment.

Our technique is sensitive to the initial few femtoseconds after the electronic change (e.g., photoionization) that drives the motion of the protons toward a new equilibrium position. In contrast, conventional methods only provide data for the potential energy surface around the equilibrium position and do not access the extremely fast proton rearrangement that follows directly from electronic changes. Our technique may therefore provide new insights into some of the most fundamental events in chemistry.

References and Notes

1. H. Niikura *et al.*, *Nature* **417**, 917 (2002).
2. H. Niikura *et al.*, *Nature* **421**, 826 (2003).
3. R. Kienberger *et al.*, *Nature* **427**, 817 (2004).
4. Y. Mairesse *et al.*, *Science* **302**, 1540 (2003).
5. P. B. Corkum, *Phys. Rev. Lett.* **71**, 1994 (1993).
6. A. L'Huillier, L.-A. Lompré, G. Mainfray, C. Manus, in *Atoms in Intense Laser Fields*, M. Gavrila, Ed. (Academic Press, New York, 1992), pp. 139–201.
7. M. Lein, *Phys. Rev. Lett.* **94**, 053004 (2005).
8. P. Antoine, A. L'Huillier, M. Lewenstein, *Phys. Rev. Lett.* **77**, 1234 (1996).
9. Y. Liang, S. Augst, S. L. Chin, Y. Beaudoin, M. Chaker, *J. Phys. B* **27**, 5119 (1994).
10. See supporting material on *Science* Online.
11. M. Lein, N. Hay, R. Velotta, J. P. Marangos, P. L. Knight, *Phys. Rev. Lett.* **88**, 183903 (2002).
12. H. Stapelfeldt, H. Sakai, E. Constant, P. B. Corkum, *Phys. Rev. Lett.* **79**, 2787 (1997).
13. M. Lein, N. Hay, R. Velotta, J. P. Marangos, P. L. Knight, *Phys. Rev. A* **66**, 023805 (2002).
14. C. J. Latimer, K. F. Dunn, F. P. O'Neill, M. A. Macdonald, N. Kouchi, *J. Chem. Phys.* **102**, 722 (1995).
15. J. Itatani *et al.*, *Nature* **432**, 867 (2004).
16. C. J. Latimer, R. A. Mackie, A. M. Sands, N. Kouchi, K. F. Dunn, *J. Phys. B* **32**, 2667 (1999).
17. R. F. Frey, E. R. Davidson, *J. Chem. Phys.* **88**, 1775 (1988).
18. Z. Vager *et al.*, *Phys. Rev. Lett.* **57**, 2793 (1986).
19. L. B. Knight, J. Steadman, D. Feller, E. R. Davidson, *J. Am. Chem. Soc.* **106**, 3700 (1984).

20. We thank J. Lazarus and M. Hohenberger for assistance with the interferometric measurements of the gas densities; L. Chipperfield, P. L. Knight, R. Torres, and C. Latimer for valuable scientific discussions; and P. Ruthven, A. Gregory, and B. Ratnasekara for technical assistance. Supported by the Research Councils UK through the Basic Technology Programme and the Engineering and Physical Sciences Research Council.

Supporting Online Material

www.sciencemag.org/cgi/content/full/1123904/DC1
Materials and Methods
Fig. S1
References

15 December 2005; accepted 13 February 2006
Published online 2 March 2006;
10.1126/science.1123904
Include this information when citing this paper.

Downloaded from http://science.sciencemag.org/ on November 19, 2019

Science

Probing Proton Dynamics in Molecules on an Attosecond Time Scale

S. Baker, J. S. Robinson, C. A. Haworth, H. Teng, R. A. Smith, C. C. Chirila, M. Lein, J. W. G. Tisch and J. P. Marangos

Science **312** (5772), 424-427.
DOI: 10.1126/science.1123904originally published online March 2, 2006

ARTICLE TOOLS http://science.sciencemag.org/content/312/5772/424

SUPPLEMENTARY MATERIALS http://science.sciencemag.org/content/suppl/2006/03/01/1123904.DC1

RELATED CONTENT http://science.sciencemag.org/content/sci/312/5772/373.full

REFERENCES This article cites 17 articles, 1 of which you can access for free
http://science.sciencemag.org/content/312/5772/424#BIBL

PERMISSIONS http://www.sciencemag.org/help/reprints-and-permissions

Use of this article is subject to the Terms of Service

Science (print ISSN 0036-8075; online ISSN 1095-9203) is published by the American Association for the Advancement of Science, 1200 New York Avenue NW, Washington, DC 20005. The title *Science* is a registered trademark of AAAS.

American Association for the Advancement of Science

Downloaded from http://science.sciencemag.org/ on November 19, 2019